HHS Public Access

Author manuscript

ACS Chem Neurosci. Author manuscript; available in PMC 2022 June 24.

Published in final edited form as:

ACS Chem Neurosci. 2022 April 20; 13(8): 1232–1244. doi:10.1021/acschemneuro.1c00847.

Europium-doped cerium oxide nanoparticles for microglial Aβ clearance and homeostasis

Jatin Machhi[1,**,#], **Pravin Yeapuri**[2,#], **Milica Markovic**[1], **Milankumar Patel**[1], **Wenhui Yan**[2], **Yaman Lu**[1], **Jacob D. Cohen**[1], **Mahmudul Hasan**[3], **Mai Mohamed Abdelmoaty**[3,4], **You Zhou**[5], **Huangui Xiong**[1], **Xinglong Wang**[1], **R. Lee Mosley**[1], **Howard E. Gendelman**[1], **Bhavesh D. Kevadiya**[1,*]

[1]Department of Pharmacology and Experimental Neuroscience, University of Nebraska Medical Center, Omaha, NE 68198, USA

[2]Department of Pharmacology, School of Basic Medical Science, Xi'an Jiaotong University Health Science Center, Xi'an, Shaanxi, 710061, China

[3]Department of Pharmaceutical Sciences, College of Pharmacy, University of Nebraska Medical Center, NE 68198, USA

[*]**Corresponding authors** Dr. Bhavesh Kevadiya, Department of Pharmacology and Experimental Neuroscience, University of Nebraska Medical Center, Omaha, NE 6898-5880; phone 402-552-7617, bhaveshd.kevadiya@unmc.edu. [**]Dr. Jatin Machhi, Department of Pharmacology and Experimental Neuroscience, University of Nebraska Medical Center, Omaha, NE 6898-5880; phone 402-559-2779. jatin.machhi@unmc.edu.

[#]EQUAL CONTRIBUTIONS

JM and PY contributed equally to this work.

AUTHORS' CONTRIBUTIONS

J.M., H.E.G., B.D.K. conceived and planed experiments; J.M., P.Y., M.M., R.C., W.H., Y.L., M.M.A. performed experiments, M.P., J.D.C., B.D.K. formulated nanoparticles and performed experiments; J.M., M.M., B.D.K. prepared figures; Y.Z. captured TEM images; J.M., M.M., R.L.M., H.E.G., B.D.K. wrote the manuscript; H.X., R.L.M., H.E.G provided oversight research progress, technical support and edited the manuscript. All the authors read and approved the final content of these studies.

COMPETING INTERESTS

The authors declare that they have no competing interests.

SUPPORTING INFORMATION

Cytotoxicity of LNPs on BV2 cells. Cytotoxicity of $A\beta_{1-42}$ and LPS on BV2 cells in absence and presence of $EuCeO_2$NPs and LNPs (PDF).

[4]Therapeutic Chemistry Department, Pharmaceutical and Drug Industries Research Division, National Research Centre, Giza, Egypt

[5]Center for Biotechnology, University of Nebraska-Lincoln, Lincoln, NE 68588, USA

Abstract

Alzheimer's disease (AD) is the most common neurodegenerative disorder. Pathologically, it is characterized by the deposition of amyloid beta (Aβ) plaques and presence of neurofibrillary tangles. These drive microglia neuroinflammation and consequent neurodegeneration. While the means to affect Aβ plaque accumulation was achieved how it affects disease outcomes remains uncertain. Cerium oxide (CeO_2) reduces Aβ plaques, oxidative stress, inflammation, and Alzheimer's disease (AD) signs and symptoms. Specifically, CeO_2 nanoparticles (CeO_2NPs) induces free radical scavenging and cell protective intracellular signaling. This can ameliorate the pathobiology of an AD-affected brain. In order to investigate, CeO_2NPs affects for microglia neurotoxic responses a novel formulation of europium doped CeO_2NPs ($EuCeO_2$NPs) was synthesized. We then tested $EuCeO_2$NPs for its' abilities to generate cellular immune homeostasis in AD models. $EuCeO_2$NPs attenuated microglia BV2 inflammatory activities after $Aβ_{1–42}$ exposure by increasing the cells' phagocytic and Aβ degradation activities. These were associated with increases in the expression of the CD36 scavenger receptor. $EuCeO_2$NPs facilitated Aβ endolysosomal trafficking and abrogated microglial inflammatory responses. We posit that $EuCeO_2$NPs may be developed as an AD immunomodulator.

Graphical Abstract

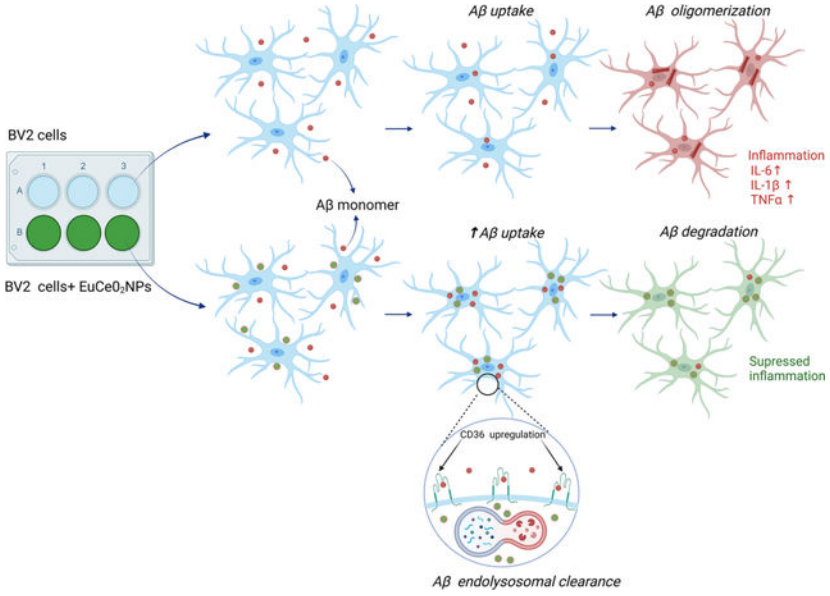

In vitro assay: $EuCeO_2$NPs treatment improves microglial phagocytosis of Aβ.

Keywords

Alzheimer's disease (AD); amyloid beta (Aβ); europium-doped cerium oxide nanoparticles ($EuCeO_2$NPs); microglia; BV2 cells and immune modulation

1. INTRODUCTION

Worldwide, Alzheimer's disease (AD) is the most common cause of age-related dementia, ranking sixth among the causes of death[1, 2]. Management costs for affected individuals are considerable and expected to raise to $20 trillion by 2030[3]. Pathologically, AD is characterized by the deposition of phosphorylated tau "tangles" and senile "plaques", the latter containing a central core of amyloid beta (Aβ) surrounded by abnormal neural processes. Both neurofibrillary tangles (NFTs) and Aβ plaques are associated with sustained neuroinflammation [2, 4], identified as a key disease driver instigated by altered innate microglial immune responses [2, 5, 6]. Under homeostatic conditions, microglia serve to clear cellular waste and protect neurons from external toxic stimuli [5, 7]. Like peripheral macrophages, microglia can acquire differential phenotypes. Depending upon the disease stage, microglia can attain a classically activated M1 phenotype (pro-inflammatory) or an alternatively activated M2 phenotype (anti-inflammatory) [2, 8]. However, recent studies support the notion that microglia phenotypes are not absolute and that they hold combinations of M1 and M2 phenotypes encompassing a spectrum of activities and intensities [9]. Additionally, microglial functions change during physiological and diseased conditions and are clearly affected by the local brain microenvironment [10]. Therefore, while microglia can be both anti-inflammatory and pro-inflammatory, a more accurate representation of the cell's function is adaptive. During the disease onset, microglia possess an anti-inflammatory phenotype, secretes neurotrophic factors, and clears debris, to facilitate central nervous system (CNS) homeostasis. This occurs, in parallel, through phagocytosis and clearance of toxic misfolded Aβ protein aggregates. Overall, they function in a neuroprotective capacity [11]. However, as diseases progresses, microglia are pro-inflammatory, becoming reactive cells that facilitates excess Aβ deposition and hyperphosphorylation of tau accelerating neurodegeneration [11, 12]. Therefore, treatments should accelerate the removal of neurotoxic Aβ deposits and interdict NFT formation. This would facilitate the anti-inflammatory and a neuroprotective state [5, 13].

Due to the complex interplay between the accumulation of aggregated misfolded proteins, neuroinflammation, and neurodegeneration therapeutic successes remain limited. Indeed, as of today, only four drugs (donepezil, rivastigmine, galantamine, memantine) are approved by the US Food and Drug Administration (U.S. FDA) for AD treatment and all provide only symptomatic relief of disease signs and symptoms [14]. A number of vaccines, antibodies and immunomodulatory agents have been developed and tested, but each have shown limitations in therapeutic outcomes or in inherent toxicities [15]. One example is aducanumab, an anti-Aβ antibody, that selectively targets aggregated forms of amyloid. Clinical follow-ons during phase 3 trials in AD patients with mild cognitive impairments have shown modest reductions in Aβ load with limited affect on cognition. The failure to demonstrate clinical benefit has compromised aducanumab utility [16]. Therefore, safer, more effective therapeutic alternatives are sorely needed. One promising approach is one designed to restore the microglial homeostatic functions and eliminate Aβ deposits. To this end, we investigated cerium, a rare earth metal which exists as oxide (CeO_2 and Ce_2O_3) in the nature, as a possible treatment based on its antioxidant functions. At an atomic level, cerium oxide is composed of Ce^{+3} and Ce^{+4} mixtures. When present

on the surface of nanoparticles and with decreasing particle size, the number of Ce^{+3} surface sites increase, and oxygen atoms are lost [17]. Due to such unique physicochemical property, CeO_2 nanoparticles (CeO_2NPs) neutralize reactive oxygen/nitrogen species. These include, but are not limited to, superoxide, nitric oxide and peroxynitrile. Indeed, CeO_2 holds biomimetic functions. It can act in the same scavenger capacity as endogenous enzymes such as catalase or superoxide dismutase (SOD) [18]. CeO_2NPs offer promising properties including ultra-small diameter that allows passage through the blood-brain-barrier (BBB), control of neurotoxic cell signaling, and potent free radical neutralizing features in divergent tissues[19, 20]. Prior works demonstrated neuroprotective effects of CeO_2NPs [21, 22]. Here, we assessed the immunomodulatory potential of europium (Eu)-doped CeO_2NPs ($EuCeO_2$NPs) in BV2 microglia cells to mimic human AD. $EuCeO_2$NPs were synthesized and characterized to achieve favorable physicochemical properties followed by co-culture with BV2 cells and Aβ. $EuCeO_2$NPs improved Aβ phagocytic microglial capabilities and Aβ degradation. By attenuating lipopolysaccharide (LPS)-elicited pro-inflammatory microglial responses, $EuCeO_2$NPs were able to restore homeostatic anti-inflammatory and neuroprotective activities.

2. METHODS

2.1 Synthesis of $EuCeO_2$NPs

$EuCeO_2$NPs were synthesized using solvothermal reactions, followed by lipid coating for biological applications. In a typical reaction mixture ~434.22 mg of cerium (III) nitrate hexahydrate ($Ce(NO_3)_3.6H_2O$ = 1.0 mM) and ~168.99 mg of europium (III) nitrate hydrate ($Eu(NO_3)_3.H_2O$= 0.5 mM) were dissolved in a mixture of 5 mL of 1-octadecene and 1 mL of oleylamine and stirred at 80°C until dissolved [23]. A clear brownish yellow solution appeared which was transferred to a Teflon lined autoclave reactor and heated to 300°C in an oven for 3 hr followed by gradual cooling to room temperature overnight. Purification was done using ethanol wash with centrifugation and it was repeated at least three times before final dispersion of nanocrystals in chloroform. Purified brown-black nanocrystals were used for lipid coating to prevent aggregation in biological medium according to our previously published protocol [24]. In brief, thin-film hydration method was used by preparing mixture of L-α-phosphatidylcholine and DSPE-PEG_{2000} in 2:1 weigh ratio. The synthesized nanocrystals ($EuCeO_2$) were dispersed in chloroform and mixed with 2% (v/v) Tween-80 to prepare an emulsion. Chloroform was completely evaporated using rotary evaporator prior to the addition of core nanocrystals into lipid film. The lipid-nanocrystal mixture was dispersed by constant rotation on bath sonicator. The lipid-coated nanocrystals were centrifuged, and particle size distribution was analyzed by dynamic light scattering instrument. The lipid nanoparticles (LNPs) without cerium oxide were used as control to ensure that the observed effects were solely attributed to the $EuCeO_2$NPs. The control LNPs were prepared using same technique except core $EuCeO_2$ nanocrystals with equivalent lipid composition and concentrations to lipid incased $EuCeO_2$NPs.

2.2 BV2 cytotoxicity and 3-(4,5-dimethylthiazol-2-yl)-2,5-diphenyltetrazolium bromide (MTT) measurements

BV2 cells were cultured in Dulbecco's modified Eagle's medium (DMEM) supplemented with (10% V/V) fetal bovine serum (FBS), 100 U/ml penicillin and 100 U/ml streptomycin at 37°C and 5% CO_2 in 75 cm^2 flasks. For the MTT assay, cells were seeded in 96-well plates at the density of 2×10^4 cells per well and incubated for 24 hr before starting the experiment. At the start of the experiment, BV2 cells were serum-starved for 4 hr followed by replacement of growth media with fresh media (control cells) or with media supplemented with increasing concentrations of $EuCeO_2$NPs (10 ng/ml to 1 μg/ml cerium equivalent weight) or with LNPs (equal volume as test particles) at 1 and 4 hrs. After incubation, cell viability was assessed using the MTT assay [25]. Briefly, 20 μl of MTT (Catalog no. M2128, Sigma Aldrich, St. Lois, MO) solution (5 mg/ml) was added into each well and incubated for 4 hr at 37°C. The culture media was replaced with 200 μl dimethyl sulfoxide (DMSO) to dissolve formazan crystals and optical density was measured at 570 nm with 630 nm reference wavelengths using Synergy™Mx Microplate Reader (BioTek, Winooski, VT). Absorbance of control cells was considered as 100% of cell viability, and $EuCeO_2$NPs and LNPs treated BV2 cell viability was calculated compared to control cells.

2.3 $A\beta_{1-42}$ and $EuCeO_2$NPs treatments

$A\beta_{1-42}$ peptide was purchased commercially (Catalog no. RP10017, GenScript, Piscataway, NJ) and $A\beta_{1-42}$ monomers were prepared according to our previous reports [26]. Briefly, $A\beta_{1-42}$ was dissolved in cold hexafluoro-2-propanol (Catalog no. 52517, Sigma Aldrich, St. Lois, MO) and incubated at room temperature for 1 hr. Hexafluoro-2-propanol evaporated during incubation and $A\beta_{1-42}$ peptide was stored as a film at −20°C. $A\beta_{1-42}$ monomer was prepared by dissolving $A\beta_{1-42}$ film in anhydrous DMSO (final concentration 2%) followed by dilution in DMEM and was immediately used in studies. Since $A\beta_{1-42}$ monomers are effectively phagocytized by macrophages and microglia compared to oligomeric $A\beta_{1-42}$ [13, 27], monomeric $A\beta_{1-42}$ was used at the final concentration of 10 μM. For follow on experiments, BV2 cells were treated with either $EuCeO_2$NPs (100 ng/ml) or LNPs for 1 hr followed by media replacements containing monomeric $A\beta_{1-42}$ (10 μM) without washing. Cultures were incubated for 1 or 4 hr for Aβ phagocytosis and degradation studies. Effects of $A\beta_{1-42}$ (10 μM) on BV2 cell viability and inflammatory responses were studied in parallel experiments.

2.4 Flow cytometry

BV2 cells seeded in 12 well plates (5×10^5/well) were serum starved for 4 hr, followed by treatment with 100 or 500 ng/ml $EuCeO_2$NPs for 1 and 4 hr. Following incubation, cells were washed and scrapped in flow staining buffer (2% FBS in phosphate buffer saline (PBS)) then examined by flow cytometry. The analysis was completed with a LSRFortessa™ flow cytometer (BD Biosciences, San Jose, CA) and data analyzed using BD FACSDiva™ software v8 (BD Biosciences, San Jose, CA) [28]. $EuCeO_2$NPs were detected using excitation with UV laser 355nm with 60.4mw power and emission with a 615/24 bandpass filter. All analysis gates were applied in order to eliminate debris, dead cells and

doublets. Untreated and LNP treated cells were used as controls as well as for precise gating of $EuCeO_2$NPs cellular uptake.

2.5 Nanoparticle characterizations

The morphology, lattice crystal structure, elemental composition, and chemical color mapping of the synthesized nanoparticles were determined by bright field high-resolution transmission electron microscopy (HR-TEM), selected area electron diffraction (SAED), energy-dispersive x-ray spectroscopy (EDX), and scanning transmission electron microscopy (STEM) with high-angle annular dark-field (HAADF) (FEI Tecnai Osiris S/TEM operated at 200 kV)[24]. Briefly, for HR-TEM, $EuCeO_2$ crystals were prepared in chloroform and dried on a copper grid at room temperature. The additional speed gain was used to collect EDX elemental mappings from a larger field-of-view. The lattice fringes of the obtained samples and the corresponding SAED patterns were examined by HR-TEM. Size of lipid coated particles was determined by hydrodynamic diameter and particle size distribution measurements in water by dynamic light scattering (Malvern Nano-Series Zetasizer system). Ceria and europium quantifications were performed by inductively coupled plasma-mass spectrometry (ICP-MS) by an Agilent 7500cx ICP-MS (Santa Clara, CA, USA) system.

2.6 Transmission electron microscopy (TEM)

For TEM, BV2 cells were seeded at a density of 1.5×10^6 cells/well in a six well plate. Cells were treated with $EuCeO_2$NPs (100 ng/ml) for 1 or 4 hr. Untreated BV2 cells served as controls. After incubation, cells were washed with PBS, and incubated in a fixative buffer containing 2% glutaraldehyde and 2% paraformaldehyde (PFA) in 0.1 M Sorenson's phosphate buffer (pH 6.2) for 1 hr at 4°C. Finally, cells were scrapped and centrifuged at 650g for 10 min and the cell pellet was resuspended in the same fixative buffer and stored at 4°C for TEM analysis [29]. Briefly, fixed cells were washed three times with 0.1 M phosphate buffer and post-fixed in 1% osmium tetroxide in deionized water for 30 min. Samples were then dehydrated in an ethanol series (50, 70, 90, 95, and 100%). After solvent transition with ethanol and Spurr's resin (50:50 ethanol:resin, followed by twice immersion in 100% Spurr's resin for 2–3 hr for each solution), samples were embedded in Spurr's resin and cured at 60°C for 36 hr. Ultrathin sections (80–90 nm) were cut with Leica UC7 ultramicrotome, placed on 200-mesh copper grids, followed by staining with 2% uranyl acetate and Reynold's lead citrate. The stained sections were examined with a Hitachi H7500 TEM at 80 kV. Images were acquired digitally with an AMT digital imaging system.

2.7 Immunofluorescence and confocal microscopy

For confocal microscopy, BV2 cells were plated at the density of 2×10^5 cells/well in a 24 well plate with a glass coverslip. BV2 cells were serum starved for 4 hr prior to $EuCeO_2$NPs (100 ng/ml) or LNPs treatment for 1 hr. Following nanoparticle treatment, media containing $A\beta_{1–42}$ (10 μM) was replaced without washing and incubated with the BV2 cells for an additional 1 hr. After $A\beta_{1–42}$ treatment, BV2 cells were fixed with 4% PFA (at neutral pH in PBS) for 15 min. The immunofluorescence staining was performed with pan-Aβ (1:500, rabbit polyclonal, Catalog no. 715800, Thermo Fisher Scientific, Waltham, MA) and Alexa Fluor 488-conjugated anti-rabbit IgG (1:500, Thermo Fisher Scientific,

Waltham, MA) antibodies, followed by Vectashield-4′,6-diamino-2-phenyl-indole (DAPI) treatments (Catalog no. PK-6100, Vector Laboratories, Burlingame, CA). DAPI was used as a blue-fluorescent DNA stain to enhance fluorescence upon binding to AT regions of dsDNA. This was completed after 30 min then counterstained and mounted. In replicate experiments, PFA-fixed BV2 cells were immunostained with Aβ (6E10, 1:1000, Catalog no. 803001, Biolegend, San Diego, CA), lysosomal-associated membrane protein 1 (Lamp1, 1:500, rat monoclonal, Catalog no. ab25245, Abcam, Cambridge, United Kingdom) and Ras-related protein 7 (Rab-7, 1:500, rabbit polyclonal, Catalog no. SC271608, Santa Cruz Biotechnology, Dallas, TX) antibodies, followed by Alexa Fluor 488-conjugated anti-mouse IgG and Alexa Flour 568-conjugated anti-rabbit IgG secondary antibody staining (1:500, Thermo Fisher Scientific, Waltham, MA) and DAPI stained. The fluorophore-conjugated IgG isotype antibody and fluorescence minus one (FMO) staining were used as background controls. Confocal images were captured using a 63X oil lens on a LSM900 confocal microscope (Carl Zeiss Microimaging Inc., White Plains, NY) and fluorescence intensities were quantified using ImageJ software (National Institute of Health).

2.8 Western blot analysis

For Western blot tests, $EuCeO_2$NPs (100 ng/ml), LNPs, and $A\beta_{1–42}$ (10 μM) treated BV2 cells were harvested in ice-cold radioimmunoprecipitation (RIPA) buffer containing protease and phosphatase inhibitors (Catalog no. 89901, Thermo Fisher Scientific, Waltham, MA). Cells were centrifuged at 15,000×g for 10 min at 4°C and supernatants collected for total protein quantification with the Micro BCA Protein assay kit (Catalog no. 23235, Thermo Fisher Scientific, Waltham, MA). Protein samples were incubated with Laemmli sample buffer containing β-mercaptoethanol at 100°C for 5 min, followed by electrophoresis on sodium dodecyl sulfate (SDS)-polyacrylamide gel. The separated proteins were transferred from gel to 0.45 μm pore-size polyvinylidene fluoride membrane (Immobilon-P, Catalog no. IPVH00010, Millipore, Burlington, MA). Later, membranes were blocked with 5% skim milk/Tris-buffered saline-Tween 20 (TBST) and incubated with primary antibodies against CD36 (1:200, Catalog no. SC7309, Santa Cruz Biotechnology, Dallas, TX), Aβ (6E10, 1:1000, Catalog no. 803001, Biolegend, San Diego, CA) and β-actin (1:2000, Catalog no. A3854, Sigma Aldrich, St. Lois, MO) at 4°C overnight, followed by 60 min incubation in 5% skim milk/TBST with horseradish peroxidase-conjugated anti-rabbit or -mouse secondary antibodies (1:2000, Santa Cruz Biotechnology, Dallas, TX). Immunoreactive bands were detected using SuperSignal West Pico or Femto Chemiluminescent substrate, and images were captured using an iBlot750 Imager (Thermo Fisher Scientific, Waltham, MA). Immunoblots were quantified using ImageJ software (National Institutes of Health) relative to β-actin expression.

2.9 Enzyme-linked immunosorbent assay (ELISA)

For $A\beta_{1–42}$ quantification, BV2 cells were pre-treated with $EuCeO_2$NPs (100 ng/ml) or LNPs for 1 hr followed by $A\beta_{1–42}$ (10 μM) exposure for 4 hr. After incubation, BV2 cells were lysed using ice-cold RIPA buffer containing protease and phosphatase inhibitors. Cell supernatants containing total protein were subjected to $A\beta_{1–42}$ ELISA (Catalog no. KHB3442, Life Technologies, Carlsbad, CA).

2.10 Quantitative real-time polymerase chain reaction (RT^2-qPCR)

To determine the effects of $EuCeO_2$NPs on microglial inflammatory responses, BV2 cells were pre-treated with $EuCeO_2$NPs (100 ng/ml) or LNPs for 1 hr followed by treatment with LPS (0.5 μg/ml) for another 4 hr. Following incubation, total RNA from BV2 cells treated with either $EuCeO_2$NPs or LNPs, was extracted using RNAeasy mini kit (Catalog no. 74104, Qiagen, Germantown, MD). The RNA was reverse transcribed into complementary DNA (cDNA) using RevertAid First Strand cDNA Synthesis kit (Catalog no. K1622, Thermo Fisher Scientific, Waltham, MA) and RT^2-qPCR primer assay was performed on a QuantStudio™ 3 Real-Time PCR System (Thermo Fisher Scientific, Waltham, MA) using 2x AzuraQuant™ Green Fast qPCR mix (Catalog no. AZ-2305, Realtimeprimers, Melrose Park, PA) and gene specific primers against mouse interleukin (IL)-6, IL-1β, IL-4, tumor necrosis factor alpha (TNF-α), interferon gamma (IFN-γ), and inducible nitric oxide synthase (iNOS) (Realtimeprimers, Melrose Park, PA). The thermocycler conditions used were 95°C for 2 min, followed by 45 cycles of 95°C for 10 sec and 58°C for 45 sec and a melting curve. Glyceraldehyde-3-phosphate dehydrogenase (GAPDH) was used as an internal control and relative expression of target genes was determined using $2^{-\Delta\Delta Ct}$ method.

2.11 Statistical analysis

All data were presented as mean ± standard error of mean (SEM). Comparisons of means between groups were analyzed by one-way ANOVA followed by Newman–Keuls post-hoc test using statistics software (GraphPad Prism version 9.2). A value of $p < 0.05$ was regarded as significant.

3. RESULTS

3.1 $EuCeO_2$NPs synthesis and characterization

We used the solvothermal method to synthesize particles with cerium and europium precursors in organic solutions to form ultra-small nanocrystals with spherical shapes. The reaction began with the full dispersion of metal precursors in a high boiling point and inert organic solvent, in this case 1-octadecene with amine surfactants as oleylamine to prevent aggregation and enhance colloidal stabilization. At high temperature, the metal precursors started nucleation and ultimately formed crystallites. The purified nanocrystals were concentrated by repeated washes with ethanol followed by cycles of centrifugation and dispersion to form monodispersed nanoparticles of relatively uniform size as demonstrated by TEM (Figure 1A). First, we performed HR-TEM analysis of synthesized $EuCeO_2$NPs to determine crystalline structure. The lattice fringes in the HR-TEM image demonstrates a crystalline structure of $EuCeO_2$NPs with a plane-to-plane distance of 0.37 nm (Figure 1B). This corresponded to a bulk ceria material space group (111) = 0.31 nm [30] and confirmed by SAED with a specific ring pattern (Figure 1C).

Second, we assessed metal ion distribution within the core particles ($EuCeO_2$) using elemental distribution energy-dispersive X-ray analysis (EDX) and found homogeneous distribution of Ce and Eu, confirmed successful formulation of $EuCeO_2$NPs (Figure 1D–F). The EDX spectrum of $EuCeO_2$NPs showed 18.13% Eu incorporated in Ce lattice (Figure 1G). The dynamic light scattering (DLS) analysis showed size distribution of lipid encased

$EuCeO_2$NPs from 100 to 300 nm with average size ~159 nm and polydispersity index (PDI) 0.04 as presented in Figure 1H, suggested formulation of monodispersed $EuCeO_2$NPs.

3.2 $EuCeO_2$NPs cytotoxicity measurements

To determine the appropriate concentrations of $EuCeO_2$NPs to use in microglia, BV2 cells were treated with varied concentrations of $EuCeO_2$NPs and equivalent LNPs for different times. Significant cytotoxicity was not observed by BV2 cells for $EuCeO_2$NPs up to 250 ng/ml for a 1 hr incubation (Figure 2A). Moreover, no cytotoxicity was recorded for $EuCeO_2$NPs at concentration of up to 100 ng/ml after a 4 hr incubation. BV2 cytotoxicity was recorded by LNPs (without Eu and CeO_2) at 250 ng/ml after 1 and 4 hr incubation (Figure S1). Based on these results, we used 100 ng/ml concentration of $EuCeO_2$NPs and control LNPs during testing of Aβ co-cultures. *First*, monomeric $A\beta_{1–42}$ (10 μM) cultured with BV2 cells for 4 hr did not induce cytotoxicity. (Figure S2A). Moreover, pre-treatment with $EuCeO_2$NPs or LNPs at a concentration of 100 ng/ml for 1 hr followed by $A\beta_{1–42}$ (10 μM) for 4 hr also did not induce BV2 cytotoxicity (Figure S2A). We showed that small sized (~160 nm) $EuCeO_2$NPs were readily taken up by BV2 cells. $EuCeO_2$NPs were detected by flow cytometric analysis using the fluorescence properties of europium covalently conjugated to CeO_2. The uptake evaluated by flow cytometric analysis of the $EuCeO_2$NPs at 100 ng/ml showed 3.7% and 12% particle uptake at 1 and 4 hr in BV2 cells (Figure 2B).

Higher $EuCeO_2$NPs uptake was observed by increasing concentration (500 ng/ml) with reductions in MTT activity (~78% viability). Thus, it should be noted that this concentration might be more toxic, can affect membrane permeability and allow more particles enter the cell. Flow cytometric results were also quantified for fluorescence intensity of europium (Figure 2C). Dose- and time-dependent increases in the fluoresce intensity were observed in $EuCeO_2$NPs treated BV2 cells compared to untreated cells. To note, europium exhibited weak fluorescence properties in cells during initial low $EuCeO_2$NP uptake; at the same time, $EuCeO_2$NP uptake by BV2 cells was not easily detected by confocal microscopy (data not shown). TEM confirmed $EuCeO_2$NP uptake as shown by nanoparticles observed within the cytoplasm in almost 50% cells within an hour after treatment (Figure 3A). After 1 hr, $EuCeO_2$NPs were taken up by BV2 cells via phagocytosis which is clearly shown in Figure 3B in red square. Generally, phagocytosis is considered as a primary mechanism for nanoparticle uptake by innate immune cells such as macrophages and microglia and is initiated immediately after contact of nanoparticles [31]. Untreated or LNPs treated BV2 cells showed similar ultrastructures indicating that LNP-treatment does not perturb non-phagocytic microglial architecture (Figure 3A).

3.3 $EuCeO_2$NPs induce Aβ BV2 phagocytosis

Microglia protect the CNS by phagocytosis of cellular debris and misfolded protein aggregates such as Aβ [5, 7]. To test the effects of $EuCeO_2$NPs on Aβ internalization, $EuCeO_2$NP pre-treated BV2 cells were exposed to monomeric $A\beta_{1–42}$ and assessed by fluorescence microscopy. We showed that $A\beta_{1–42}$ was readily taken up by BV2 cells within 1 hr of treatment (Figure 4A). However, $EuCeO_2$NPs facilitated $A\beta_{1–42}$ uptake while control LNPs treatment alone did not potentiate $A\beta_{1–42}$ uptake. Quantitative analysis

of Aβ fluorescence intensity by digital image analysis showed significant amyloid entry into BV2 cells by $EuCeO_2$NPs ($p < 0.05$) compared to $A\beta_{1–42}$ alone, or control LNPs and $A\beta_{1–42}$ treated cells (Figure 4B). As microglial phagocytic activities are attributed to scavenger receptors expressed on the cell surface [32], we studied the role of the key scavenger receptor, CD36 in microglial uptake of Aβ after treatment of BV2 cells with $EuCeO_2$NPs, LNPs, and/or $A\beta_{1–42}$. We observed that LNPs alone had no effect, whereas $A\beta_{1–42}$ treatment significantly upregulated CD36 expression compared to untreated controls ($p<0.01$) (Figure 4C), thus linking scavenger receptor upregulation to uptake of Aβ. Surprisingly, LNP treatment reduced $A\beta_{1–42}$-mediated CD36 expression, although the difference was not significant. In contrast, $EuCeO_2$NPs and $EuCeO_2$NPs plus $A\beta_{1–42}$, increased CD36 expression when compared to $A\beta_{1–42}$ alone ($p < 0.05$). No differences in CD36 expression was observed between $EuCeO_2$NPs and $EuCeO_2$NPs and $A\beta_{1–42}$ highlighting potential of $EuCeO_2$NPs to induce optimum scavenger receptor expression itself in BV2 cells. Overall, $EuCeO_2$NPs promoted $A\beta_{1–42}$ phagocytosis in BV2 cells that was associated with scavenger receptor upregulation.

3.4 $EuCeO_2$NPs localize Aβ in endolysosomal compartments

Microglial phagocytosis involves the endolysosomal pathway, where engulfed molecules are being trafficked for further degradation and clearance [33, 34]. After Aβ binds to scavenger receptors, microglia initiate phagocytosis and unload Aβ into endosomal and lysosomal compartments [2, 13].

Therefore, we evaluated the effects of $EuCeO_2$NPs on Aβ endolysosomal trafficking following phagocytosis. One-hour post-treatment, Aβ was localized in late endosomal (Rab7) (Figure 5A) and lysosomal (LAMP-1) (Figure 5B) compartments of BV2 cells. However, $EuCeO_2$NP pre-treatment of BV2 cells showed higher expression of Aβ that co-localized with Rab7 and LAMP1 (indicated by red arrow); this contrasted BV2 cells pre-treated with LNPs, which showed Aβ expression equivalent to cells treated with $A\beta_{1–42}$ alone. These results demonstrated the ability of $EuCeO_2$NPs to traffic more Aβ in endosomal and lysosomal compartments for disposal.

3.5 $EuCeO_2$NPs facilitate Aβ metabolism

Aβ monomers are highly susceptible to aggregation leading to the formation of soluble oligomers ranging from dimer to tetramer to prefibrillar structures [35]. Once misfolded protein aggregates are delivered to lysosomal compartment, they are metabolized and ultimately cleared [33, 36]. BV2 cells, 4 hr post-$A\beta_{1–42}$ monomer treatment, showed expression of 2-, 4-, 5-, 9- and 12-mers, as demonstrated by immunoblots (Figure 6A, top-lower and bottom-higher exposure). This is supportive of the predilection that microglia mediate Aβ oligomerization. Similarly, oligomerization of Aβ was exhibited by LNP-treated BV2 cells.

However, densitometric analysis revealed that $EuCeO_2$NP treatment of BV2 cells reduced 4-, 5-, 9-mers ($p < 0.05$), and 12-mers (trends but not significant) compared to cells treated with $A\beta_{1–42}$ alone (Figure 6B). Like Western blot analysis, ELISA assessment showed that Tris-HCl soluble $A\beta_{1–42}$ levels were significantly reduced from $EuCeO_2$NP treated cells

compared to those treated with $A\beta_{1–42}$ alone ($p < 0.05$) (Figure 6C). Overall, these results confirmed that $EuCeO_2$NPs can facilitate Aβ clearance in BV2 cells.

3.6 $EuCeO_2$NPs attenuate microglia inflammation

Microglia activation is a key mechanism of AD-linked neurodegeneration, which is an outcome associated with the imbalance between pro- and anti- inflammatory phenotypes [2, 4]. To determine the ability of $A\beta_{1–42}$ to induce microglia activation, expression of different pro-inflammatory cytokines including IL-6, IL-1β and TNF-α was assessed using RT^2-qPCR primer assays. Surprisingly, neither 1 nor 4 hr treatment of $A\beta_{1–42}$ induced significant upregulation of pro-inflammatory cytokines in BV2 cells compared to the untreated control cells, different from primary microglia [13, 37]. The results suggest reduced pro-inflammatory cytokine expression by BV2 cells [38]. BV2 cell treatment with $EuCeO_2$NPs or LNPs, either alone or with Aβ did not induce pro-inflammatory cytokines and levels were similar to the untreated control BV2 cells. LPS levels are elevated in AD patients activate microglia by toll-like receptors (TLRs), initiate an inflammatory cascade, induce innate immune responses, and lead to neurodegeneration [39].

BV2 cells were treated with LPS to recapitulate the microglial inflammatory responses seen during disease. LPS alone or in the presence of $EuCeO_2$NPs was not cytotoxic (Figure S2B). LPS treatment led to an upregulation of IL-6, IL-1β, and TNF-α (Figure 7) but IFN-γ levels were similar to the untreated control cells. LPS treated cells receiving LNP pre-treatment did not demonstrate significant differences in cytokine gene expression levels when compared to only LPS treated cells (Figure 7).

However, $EuCeO_2$NP pre-treatment significantly downregulated LPS-induced IL-6 ($p < 0.01$ and $p < 0.05$) and IL-1β ($p < 0.001$ and $p < 0.05$) compared to cells treated with LPS ± LNPs. Although not significant, $EuCeO_2$NPs also suppressed LPS-induced TNF-α gene expression by ~10% compared to the treatment with LPS ± LNPs. The classical microglial activation marker inducible nitric oxide synthase (iNOS) expression was significantly elevated after LPS treatment ($p<0.001$). In contrast, iNOS was significantly reduced by the pre-treatment of $EuCeO_2$NPs ($p<0.01$). Interestingly, LNPs pre-treatment induced iNOS expression in BV2 cells. Next, we determined the gene expression of anti-inflammatory cytokines IL-4 and IL-13 that function to suppress pro-inflammatory milieu and maintain homeostasis. No IL-13 gene induction was observed in control BV2 cells compared to LPS treated cells. However, IL-4 gene expression was significantly decreased in LPS treated BV2 microglial cells compared to the untreated control cells ($p<0.001$). Pre-treatment of $EuCeO_2$NPs significantly reverted LPS induced suppression of IL-4 gene expression ($p<0.01$) but not LNP treatment. Thus, these results suggest that $EuCeO_2$NPs attenuate pro-inflammatory microglia activation, which can in turn facilitate restoration of homeostatic phenotypes.

4. DISCUSSION

Apart from the classical pathological hallmarks, neuroinflammation has been established over the past two decades as an important exacerbating, if not etiological, factor in AD [4–6]. Microglia are unique, CNS residing, innate immune cells, which play an indispensable

role in homeostasis and neuroinflammation [5, 7]. Under physiological conditions, microglia maintain neuronal vitality, promote T cell responses, and remove cellular debris though endolysosomal activities. However, during disease progression, microglia polarize towards pro-inflammatory phenotypes with impaired phagocytic capabilities, facilitating excess Aβ deposition, neuroinflammatory cascade and neurodegeneration [11, 12]. Several therapeutic strategies have been developed to facilitate Aβ clearance using experimental animal models, including non-steroidal anti-inflammatory drugs (NSAIDs) [40], active and passive Aβ immunization [41], Aβ degrading enzymes [42], and hemodialysis of Aβ [43]. This suggests that alternative strategies to improve Aβ clearance are warranted. Restoring altered innate immune cell functions could prove to be a promising strategy to interdict amyloid deposition. One such possibility is CeO_2. Due to such potent antioxidant and free radical scavenging properties, CeO_2NPs, in particular, has emerged as a therapeutic alternative for treatment of neurodegenerative and neuroinflammatory diseases that include AD, Parkinson's disease (PD), amyotrophic lateral sclerosis (ALS), multiple sclerosis (MS) and stroke.

To design an optimum immune modulator for the treatment of AD, several factors need be considered. These include, but are not limited to, biocompatibility, BBB permeability, tissue distribution, degradation, and elimination. Generally, small molecular weight drugs require higher doses for the treatment of neurodegenerative diseases, since only a small amount of drug can cross the BBB and reach the brain, while large amounts of drug remain in the peripheral blood causing significant side effects. Nanoparticles have advantages over traditional drug molecules. For instance, their small size, with high surface-to-volume ratio favor the BBB permeability and interaction with microglia, leading to reduced systemic side effects [44]. Cerium is a unique rare-earth metal which exists in two oxidative states Ce^{+3} and Ce^{+4}, due to the presence of oxygen moieties. Nanoformulation of cerium oxides as a CeO_2NP supports the promising free radical scavenging and anti-apoptotic properties of the compound [17]. CeO_2NPs have been studied for the treatment of CNS inflammatory conditions including AD [22], PD [45] and ALS [46]. In addition, CeO_2NPs have also demonstrated protective efficacy in animal models of peripheral tissue damage including diabetes [47] and ulcerative colitis [48]. The beneficial effects of CeO_2NPs on peripheral and central inflammatory conditions are reported to be attributable to their potent free radical scavenging properties. In AD, the secondary outcomes of misfolded amyloid deposition include metal ion and free radical induction, and oxidative stress, which together contribute to neurodegenerative processes [49]. CeO_2NPs show protective effects in cell-based assays and AD models [21, 22 20, 22, 50,51].

In the present study, EuCeO_2NPs were synthesized, characterized, and their immunomodulatory activities assessed through the use of the BV2 microglia cell line. Europium conjugation of CeO_2NPs allowed cell tracking. EuCeO_2NP cellular uptake seen by flow cytometry was reflective of europium fluorescent properties. Nontoxic concentrations of EuCeO_2NPs improved microglia Aβ phagocytosis and the upregulation of scavenger receptors. CD36 is a prototypical member of scavenger receptor B family that is abundantly expressed in macrophages, microglia, and astrocytes [51]. EuCeO_2NP increased the expression of CD36 in BV2 microglia cells. After engulfment of Aβ by scavenger receptors, microglial endolysosomal pathways facilitate Aβ degradation. EuCeO_2NPs

control induction of pro-inflammatory cytokines with regulation of microglial inflammatory responses. LPS treatment mimics these events leading to increased pro-inflammatory IL-6, IL-1β, and TNF-α as well as decreased anti-inflammatory IL-4 cytokines [52]. Expression of each pro-inflammatory cytokines and classical activation marker iNOS were reduced, while anti-inflammatory cytokine increased by $EuCeO_2$NPs treatment.

Taken together, the present study serves to support the idea that $EuCeO_2$NPs correct aberrant CNS innate immune responses against the accumulation of disease-associated misfolded self-proteins such as Aβ and consequent inflammation, and as such leads to restoration of microglial homeostasis. Such effects facilitate amyloid clearance and attenuate cytotoxicity. Additional studies will determine the stage of the disease when $EuCeO_2$NPs should be used for optimal control of innate inflammatory responses and clearance of early Aβ deposits. The latter would best be accomplished before Aβ accumulation and AD progression. $EuCeO_2$NPs hold a promising place due to its unique physicochemical properties. The future deployment of primary microglia combined with studies of these nanoparticles in AD animal models will facilitate the future translational impact of $EuCeO_2$NPs.

5. CONCLUSIONS

$EuCeO_2$NPs are readily taken up by BV2 cells and facilitate phagocytosis and intracellular clearance of Aβ aggregates. $EuCeO_2$NP effects are linked to the particle's ability to polarize microglia from a pro-inflammatory to an anti-inflammatory state which facilitates cellular homeostasis. $EuCeO_2$NPs may serve as an immunomodulator for AD treatment.

Supplementary Material

Refer to Web version on PubMed Central for supplementary material.

ACKNOWLEDGEMENTS

The authors thank the Flow Cytometry Research Core Facility and Advanced Microscopy Core Facility at the University of Nebraska Medical Center for assistance with flow cytometric and confocal image analyses.

FUNDING

This work was supported by the National Institutes of Health grants P01 DA028555, R01 NS36126, P01 NS31492, P01 MH64570, P01 NS43985, P30 MH062261, R01 AG043540, and 2R01 NS034239; the Frances and Louie Blumkin and Harriet Singer Research Foundations, the Carol Swarts, MD Emerging Neuroscience Research Laboratory; and the Margaret R. Larson Professorship.

REFERENCES

(1). Machhi J; Kevadiya BD; Muhammad IK; Herskovitz J; Olson KE; Mosley RL; Gendelman HE Harnessing regulatory T cell neuroprotective activities for treatment of neurodegenerative disorders. Mol Neurodegener 2020, 15 (1), 32. DOI: 10.1186/s13024-020-00375-7. [PubMed: 32503641]

(2). Kiyota T; Machhi J; Lu Y; Dyavarshetty B; Nemati M; Zhang G; Mosley RL; Gelbard HA; Gendelman HE URMC-099 facilitates amyloid-beta clearance in a murine model of Alzheimer's disease. J Neuroinflammation 2018, 15 (1), 137. DOI: 10.1186/s12974-018-1172-y. [PubMed: 29729668]

(3). 2019 Alzheimer's disease facts and figures. Alzheimer's & Dementia 2019, 15 (3), 321–387. DOI: 10.1016/j.jalz.2019.01.010.Nichols E; Szoeke CEI; Vollset SE; Abbasi N; Abd-Allah F; Abdela J; Aichour MTE; Akinyemi RO; Alahdab F; Asgedom SW; et al. Global, regional, and national burden of Alzheimer's disease and other dementias, 1990–2016: a systematic analysis for the Global Burden of Disease Study 2016. The Lancet Neurology 2019, 18 (1), 88–106. DOI: 10.1016/S1474-4422(18)30403-4 (acccessed 2019/10/30). [PubMed: 30497964]

(4). Kiyota T; Machhi J; Lu Y; Dyavarshetty B; Nemati M; Yokoyama I; Mosley RL; Gendelman HE Granulocyte-macrophage colony-stimulating factor neuroprotective activities in Alzheimer's disease mice. J Neuroimmunol 2018, 319, 80–92. DOI: 10.1016/j.jneuroim.2018.03.009. [PubMed: 29573847]

(5). J., M.; B., K.; K., M. I.; J., H.; E., O. K.; L., M. R.; E., G. H. Harnessing regulatory T cell neuroprotective activities for treatment of neurodegenerative disorders. Mol Neurodegener 2020, In press.

(6). Heneka MT; Carson MJ; El Khoury J; Landreth GE; Brosseron F; Feinstein DL; Jacobs AH; Wyss-Coray T; Vitorica J; Ransohoff RM; et al. Neuroinflammation in Alzheimer's disease. Lancet Neurol 2015, 14 (4), 388–405. DOI: 10.1016/S1474-4422(15)70016-5. [PubMed: 25792098]

(7). Matcovitch-Natan O; Winter DR; Giladi A; Vargas Aguilar S; Spinrad A; Sarrazin S; Ben-Yehuda H; David E; Zelada Gonzalez F; Perrin P; et al. Microglia development follows a stepwise program to regulate brain homeostasis. Science 2016, 353 (6301), aad8670. DOI: 10.1126/science.aad8670. [PubMed: 27338705]

(8). Mills CD; Kincaid K; Alt JM; Heilman MJ; Hill AM M-1/M-2 macrophages and the Th1/Th2 paradigm. J Immunol 2000, 164 (12), 6166–6173. DOI: 10.4049/jimmunol.164.12.6166. [PubMed: 10843666] Tang Y; Le W Differential Roles of M1 and M2 Microglia in Neurodegenerative Diseases. Mol Neurobiol 2016, 53 (2), 1181–1194. DOI: 10.1007/s12035-014-9070-5. [PubMed: 25598354]

(9). Bottcher C; Schlickeiser S; Sneeboer MAM; Kunkel D; Knop A; Paza E; Fidzinski P; Kraus L; Snijders GJL; Kahn RS; et al. Human microglia regional heterogeneity and phenotypes determined by multiplexed single-cell mass cytometry. Nat Neurosci 2019, 22 (1), 78–90. DOI: 10.1038/s41593-018-0290-2. [PubMed: 30559476] Ransohoff RM A polarizing question: do M1 and M2 microglia exist? Nat Neurosci 2016, 19 (8), 987–991. DOI: 10.1038/nn.4338. [PubMed: 27459405] Stratoulias V; Venero JL; Tremblay ME; Joseph B Microglial subtypes: diversity within the microglial community. EMBO J 2019, 38 (17), e101997. DOI: 10.15252/embj.2019101997. [PubMed: 31373067]

(10). Ajami B; Samusik N; Wieghofer P; Ho PP; Crotti A; Bjornson Z; Prinz M; Fantl WJ; Nolan GP; Steinman L Single-cell mass cytometry reveals distinct populations of brain myeloid cells in mouse neuroinflammation and neurodegeneration models. Nat Neurosci 2018, 21 (4), 541–551. DOI: 10.1038/s41593-018-0100-x. [PubMed: 29507414] Jordao MJC; Sankowski R; Brendecke SM; Sagar; Locatelli G; Tai YH; Tay TL; Schramm E; Armbruster S; Hagemeyer N; et al. Single-cell profiling identifies myeloid cell subsets with distinct fates during neuroinflammation. Science 2019, 363 (6425). DOI: 10.1126/science.aat7554.

(11). Wang WY; Tan MS; Yu JT; Tan L Role of pro-inflammatory cytokines released from microglia in Alzheimer's disease. Ann Transl Med 2015, 3 (10), 136. DOI: 10.3978/j.issn.2305-5839.2015.03.49. [PubMed: 26207229] Mizuno T The biphasic role of microglia in Alzheimer's disease. Int J Alzheimers Dis 2012, 2012, 737846. DOI: 10.1155/2012/737846. [PubMed: 22655214]

(12). Gendelman HE; Mosley RL A Perspective on Roles Played by Innate and Adaptive Immunity in the Pathobiology of Neurodegenerative Disorders. J Neuroimmune Pharmacol 2015, 10 (4), 645–650. DOI: 10.1007/s11481-015-9639-4. [PubMed: 26520433]

(13). Dong W; Embury CM; Lu Y; Whitmire SM; Dyavarshetty B; Gelbard HA; Gendelman HE; Kiyota T The mixed-lineage kinase 3 inhibitor URMC-099 facilitates microglial amyloid-beta degradation. J Neuroinflammation 2016, 13 (1), 184. DOI: 10.1186/s12974-016-0646-z. [PubMed: 27401058]

(14). Association A. s. FDA-approved treatments for Alzheimer's. 2019, https://www.alz.org/media/documents/fda-approved-treatments-alzheimers-ts.pdf.

(15). Nicoll JA; Wilkinson D; Holmes C; Steart P; Markham H; Weller RO Neuropathology of human Alzheimer disease after immunization with amyloid-beta peptide: a case report. Nat Med 2003, 9 (4), 448–452. DOI: 10.1038/nm840. [PubMed: 12640446] Schenk D; Barbour R; Dunn W; Gordon G; Grajeda H; Guido T; Hu K; Huang J; Johnson-Wood K; Khan K; et al. Immunization with amyloid-beta attenuates Alzheimer-disease-like pathology in the PDAPP mouse. Nature 1999, 400 (6740), 173–177. DOI: 10.1038/22124. [PubMed: 10408445] Mullard A Anti-amyloid failures stack up as Alzheimer antibody flops. Nat Rev Drug Discov 2019. DOI: 10.1038/d41573-019-00064-1.Yiannopoulou KG; Anastasiou AI; Zachariou V; Pelidou SH Reasons for Failed Trials of Disease-Modifying Treatments for Alzheimer Disease and Their Contribution in Recent Research. Biomedicines 2019, 7 (4). DOI: 10.3390/biomedicines7040097.

(16). Dunn B; Stein P; Cavazzoni P Approval of Aducanumab for Alzheimer Disease-The FDA's Perspective. JAMA Intern Med 2021, 181 (10), 1276–1278. DOI: 10.1001/jamainternmed.2021.4607. [PubMed: 34254984] Perlmutter JS Aducanumab: look before leaping. Nat Med 2021, 27 (9), 1499. DOI: 10.1038/s41591-021-01477-5. [PubMed: 34413517] Sevigny J; Chiao P; Bussiere T; Weinreb PH; Williams L; Maier M; Dunstan R; Salloway S; Chen T; Ling Y; et al. The antibody aducanumab reduces Abeta plaques in Alzheimer's disease. Nature 2016, 537 (7618), 50–56. DOI: 10.1038/nature19323. [PubMed: 27582220]

(17). Dhall A; Self W Cerium Oxide Nanoparticles: A Brief Review of Their Synthesis Methods and Biomedical Applications. Antioxidants (Basel) 2018, 7 (8). DOI: 10.3390/antiox7080097.Korsvik C; Patil S; Seal S; Self WT Superoxide dismutase mimetic properties exhibited by vacancy engineered ceria nanoparticles. Chem Commun (Camb) 2007, (10), 1056–1058. DOI: 10.1039/b615134e. [PubMed: 17325804]

(18). Dahle JT; Arai Y Environmental geochemistry of cerium: applications and toxicology of cerium oxide nanoparticles. Int J Environ Res Public Health 2015, 12 (2), 1253–1278. DOI: 10.3390/ijerph120201253. [PubMed: 25625406] Dowding JM; Dosani T; Kumar A; Seal S; Self WT Cerium oxide nanoparticles scavenge nitric oxide radical (NO). Chem Commun (Camb) 2012, 48 (40), 4896–4898. DOI: 10.1039/c2cc30485f. [PubMed: 22498787]

(19). Naz S; Beach J; Heckert B; Tummala T; Pashchenko O; Banerjee T; Santra S Cerium oxide nanoparticles: a 'radical' approach to neurodegenerative disease treatment. Nanomedicine (Lond) 2017, 12 (5), 545–553. DOI: 10.2217/nnm-2016-0399. [PubMed: 28181459]

(20). Kassem LM; Ibrahim NA; Farhana SA Nanoparticle Therapy Is a Promising Approach in the Management and Prevention of Many Diseases: Does It Help in Curing Alzheimer Disease? Journal of Nanotechnology 2020, 2020, 8147080. DOI: 10.1155/2020/8147080.

(21). Heckman KL; DeCoteau W; Estevez A; Reed KJ; Costanzo W; Sanford D; Leiter JC; Clauss J; Knapp K; Gomez C; et al. Custom cerium oxide nanoparticles protect against a free radical mediated autoimmune degenerative disease in the brain. ACS Nano 2013, 7 (12), 10582–10596. DOI: 10.1021/nn403743b. [PubMed: 24266731] Dowding JM; Song W; Bossy K; Karakoti A; Kumar A; Kim A; Bossy B; Seal S; Ellisman MH; Perkins G; et al. Cerium oxide nanoparticles protect against Abeta-induced mitochondrial fragmentation and neuronal cell death. Cell Death Differ 2014, 21 (10), 1622–1632. DOI: 10.1038/cdd.2014.72. [PubMed: 24902900]

(22). Kwon HJ; Cha MY; Kim D; Kim DK; Soh M; Shin K; Hyeon T; Mook-Jung I Mitochondria-Targeting Ceria Nanoparticles as Antioxidants for Alzheimer's Disease. ACS Nano 2016, 10 (2), 2860–2870. DOI: 10.1021/acsnano.5b08045. [PubMed: 26844592]

(23). Othman A; Hayat A; Andreescu S Eu-Doped Ceria Nanocrystals as Nanoenzyme Fluorescent Probes for Biosensing. ACS Applied Nano Materials 2018, 1 (10), 5722–5735. DOI: 10.1021/acsanm.8b01345.

(24). Kevadiya BD; Ottemann B; Mukadam IZ; Castellanos L; Sikora K; Hilaire JR; Machhi J; Herskovitz J; Soni D; Hasan M; et al. Rod-shape theranostic nanoparticles facilitate antiretroviral drug biodistribution and activity in human immunodeficiency virus susceptible cells and tissues. Theranostics 2020, 10 (2), 630–656. DOI: 10.7150/thno.39847. [PubMed: 31903142]

(25). Machhi J; Prajapati N; Tripathi A; Parikh ZS; Kanhed AM; Patel K; Pillai PP; Giridhar R; Yadav MR Synthesis and Biological Evaluation of Novel Multi-target-Directed Benzazepines Against Excitotoxicity. Mol Neurobiol 2017, 54 (9), 6697–6722. DOI: 10.1007/s12035-016-0184-9. [PubMed: 27744571] Machhi J; Sinha A; Patel P; Kanhed AM; Upadhyay P; Tripathi A; Parikh ZS; Chruvattil R; Pillai PP; Gupta S; et al. Neuroprotective Potential of Novel Multi-Targeted Isoalloxazine Derivatives in Rodent Models of Alzheimer's Disease Through Activation of

Canonical Wnt/beta-Catenin Signalling Pathway. Neurotox Res 2016, 29 (4), 495–513. DOI: 10.1007/s12640-016-9598-4. [PubMed: 26797524]

(26). Kiyota T; Gendelman HE; Weir RA; Higgins EE; Zhang G; Jain M CCL2 affects beta-amyloidosis and progressive neurocognitive dysfunction in a mouse model of Alzheimer's disease. Neurobiol Aging 2013, 34 (4), 1060–1068. DOI: 10.1016/j.neurobiolaging.2012.08.009. [PubMed: 23040664] Kiyota T; Yamamoto M; Xiong H; Lambert MP; Klein WL; Gendelman HE; Ransohoff RM; Ikezu T CCL2 accelerates microglia-mediated Abeta oligomer formation and progression of neurocognitive dysfunction. PLoS One 2009, 4 (7), e6197. DOI: 10.1371/journal.pone.0006197. [PubMed: 19593388]

(27). Yamamoto M; Kiyota T; Walsh SM; Liu J; Kipnis J; Ikezu T Cytokine-mediated inhibition of fibrillar amyloid-beta peptide degradation by human mononuclear phagocytes. J Immunol 2008, 181 (6), 3877–3886. DOI: 10.4049/jimmunol.181.6.3877. [PubMed: 18768842]

(28). Mukadam IZ; Machhi J; Herskovitz J; Hasan M; Oleynikov MD; Blomberg WR; Svechkarev D; Mohs AM; Zhou Y; Dash P; et al. Rilpivirine-associated aggregation-induced emission enables cell-based nanoparticle tracking. Biomaterials 2020, 231, 119669. DOI: 10.1016/j.biomaterials.2019.119669. [PubMed: 31865227]

(29). Abdelmoaty MM; Yeapuri P; Machhi J; Olson KE; Shahjin F; Kumar V; Zhou Y; Liang J; Pandey K; Acharya A; et al. Defining the Innate Immune Responses for SARS-CoV-2-Human Macrophage Interactions. Front Immunol 2021, 12, 741502. DOI: 10.3389/fimmu.2021.741502. [PubMed: 34671355]

(30). Dvořák F; Szabová L; Johánek V; Farnesi Camellone M; Stetsovych V; Vorokhta M; Tovt A; Skála T; Matolínová I; Tateyama Y; et al. Bulk Hydroxylation and Effective Water Splitting by Highly Reduced Cerium Oxide: The Role of O Vacancy Coordination. ACS Catalysis 2018, 8 (5), 4354–4363. DOI: 10.1021/acscatal.7b04409.Ziemba M; Schilling C; Ganduglia-Pirovano MV; Hess C Toward an Atomic-Level Understanding of Ceria-Based Catalysts: When Experiment and Theory Go Hand in Hand. Accounts of Chemical Research 2021, 54 (13), 2884–2893. DOI: 10.1021/acs.accounts.1c00226. [PubMed: 34137246]

(31). Gustafson HH; Holt-Casper D; Grainger DW; Ghandehari H Nanoparticle Uptake: The Phagocyte Problem. Nano Today 2015, 10 (4), 487–510. DOI: 10.1016/j.nantod.2015.06.006. [PubMed: 26640510]

(32). Eugenin J; Vecchiola A; Murgas P; Arroyo P; Cornejo F; von Bernhardi R Expression Pattern of Scavenger Receptors and Amyloid-beta Phagocytosis of Astrocytes and Microglia in Culture are Modified by Acidosis: Implications for Alzheimer's Disease. J Alzheimers Dis 2016, 53 (3), 857–873. DOI: 10.3233/JAD-160083. [PubMed: 27258416] Yu Y; Ye RD Microglial Abeta receptors in Alzheimer's disease. Cell Mol Neurobiol 2015, 35 (1), 71–83. DOI: 10.1007/s10571-014-0101-6. [PubMed: 25149075]

(33). Sole-Domenech S; Cruz DL; Capetillo-Zarate E; Maxfield FR The endocytic pathway in microglia during health, aging and Alzheimer's disease. Ageing Res Rev 2016, 32, 89–103. DOI: 10.1016/j.arr.2016.07.002. [PubMed: 27421577]

(34). Janda E; Boi L; Carta AR Microglial Phagocytosis and Its Regulation: A Therapeutic Target in Parkinson's Disease? Front Mol Neurosci 2018, 11, 144. DOI: 10.3389/fnmol.2018.00144. [PubMed: 29755317]

(35). Tamagno E; Guglielmotto M; Monteleone D; Manassero G; Vasciaveo V; Tabaton M The Unexpected Role of Abeta1–42 Monomers in the Pathogenesis of Alzheimer's Disease. J Alzheimers Dis 2018, 62 (3), 1241–1245. DOI: 10.3233/JAD-170581. [PubMed: 29103036] Walsh DM; Tseng BP; Rydel RE; Podlisny MB; Selkoe DJ The oligomerization of amyloid beta-protein begins intracellularly in cells derived from human brain. Biochemistry 2000, 39 (35), 10831–10839. DOI: 10.1021/bi001048s. [PubMed: 10978169]

(36). Majumdar A; Cruz D; Asamoah N; Buxbaum A; Sohar I; Lobel P; Maxfield FR Activation of microglia acidifies lysosomes and leads to degradation of Alzheimer amyloid fibrils. Mol Biol Cell 2007, 18 (4), 1490–1496. DOI: 10.1091/mbc.e06-10-0975. [PubMed: 17314396]

(37). Kim HJ; Ajit D; Peterson TS; Wang Y; Camden JM; Gibson Wood W; Sun GY; Erb L; Petris M; Weisman GA Nucleotides released from Abeta(1)(−)(4)(2) -treated microglial cells increase cell migration and Abeta(1)(−)(4)(2) uptake through P2Y(2) receptor activation. J Neurochem 2012, 121 (2), 228–238. DOI: 10.1111/j.1471-4159.2012.07700.x. [PubMed: 22353164]

(38). Henn A; Lund S; Hedtjarn M; Schrattenholz A; Porzgen P; Leist M The suitability of BV2 cells as alternative model system for primary microglia cultures or for animal experiments examining brain inflammation. ALTEX 2009, 26 (2), 83–94. DOI: 10.14573/altex.2009.2.83. [PubMed: 19565166] He Y; Yao X; Taylor N; Bai Y; Lovenberg T; Bhattacharya A RNA sequencing analysis reveals quiescent microglia isolation methods from postnatal mouse brains and limitations of BV2 cells. J Neuroinflammation 2018, 15 (1), 153. DOI: 10.1186/s12974-018-1195-4. [PubMed: 29788964]

(39). Zhao Y; Cong L; Lukiw WJ Lipopolysaccharide (LPS) Accumulates in Neocortical Neurons of Alzheimer's Disease (AD) Brain and Impairs Transcription in Human Neuronal-Glial Primary Co-cultures. Front Aging Neurosci 2017, 9, 407. DOI: 10.3389/fnagi.2017.00407. [PubMed: 29311897] Zhao Y; Cong L; Jaber V; Lukiw WJ Microbiome-Derived Lipopolysaccharide Enriched in the Perinuclear Region of Alzheimer's Disease Brain. Front Immunol 2017, 8, 1064. DOI: 10.3389/fimmu.2017.01064. [PubMed: 28928740]

(40). Breitner JC; Baker LD; Montine TJ; Meinert CL; Lyketsos CG; Ashe KH; Brandt J; Craft S; Evans DE; Green RC; et al. Extended results of the Alzheimer's disease anti-inflammatory prevention trial. Alzheimers Dement 2011, 7 (4), 402–411. DOI: 10.1016/j.jalz.2010.12.014. [PubMed: 21784351] de Craen AJ; Gussekloo J; Vrijsen B; Westendorp RG Meta-analysis of nonsteroidal antiinflammatory drug use and risk of dementia. Am J Epidemiol 2005, 161 (2), 114–120. DOI: 10.1093/aje/kwi029. [PubMed: 15632261]

(41). Wisniewski T Follow-up of active Abeta immunization in Alzheimer disease. Nat Rev Neurol 2019, 15 (9), 495–496. DOI: 10.1038/s41582-019-0239-4. [PubMed: 31308505] Wisniewski T; Goni F Immunotherapeutic approaches for Alzheimer's disease. Neuron 2015, 85 (6), 1162–1176. DOI: 10.1016/j.neuron.2014.12.064. [PubMed: 25789753]

(42). Miners JS; Baig S; Palmer J; Palmer LE; Kehoe PG; Love S Abeta-degrading enzymes in Alzheimer's disease. Brain Pathol 2008, 18 (2), 240–252. DOI: 10.1111/j.1750-3639.2008.00132.x. [PubMed: 18363935] Miners JS; Barua N; Kehoe PG; Gill S; Love S Abeta-degrading enzymes: potential for treatment of Alzheimer disease. J Neuropathol Exp Neurol 2011, 70 (11), 944–959. DOI: 10.1097/NEN.0b013e3182345e46. [PubMed: 22002425]

(43). Kitaguchi N; Kato T; Matsunaga S; Hirano K; Iwata K; Kawaguchi K; Fujita K; Takechi H; Hasegawa M; Yuzawa Y; et al. Removal of blood amyloid-beta with hemodialysis reduced brain amyloid-beta, confirmed by brain imaging: a case report. Neuropsychiatr Dis Treat 2018, 14, 2931–2937. DOI: 10.2147/NDT.S186118. [PubMed: 30464477]

(44). Naqvi S; Panghal A; Flora SJS Nanotechnology: A Promising Approach for Delivery of Neuroprotective Drugs. Front Neurosci 2020, 14, 494. DOI: 10.3389/fnins.2020.00494. [PubMed: 32581676] Srikanth M; Kessler JA Nanotechnology-novel therapeutics for CNS disorders. Nat Rev Neurol 2012, 8 (6), 307–318. DOI: 10.1038/nrneurol.2012.76. [PubMed: 22526003]

(45). Hegazy MA; Maklad HM; Samy DM; Abdelmonsif DA; El Sabaa BM; Elnozahy FY Cerium oxide nanoparticles could ameliorate behavioral and neurochemical impairments in 6-hydroxydopamine induced Parkinson's disease in rats. Neurochem Int 2017, 108, 361–371. DOI: 10.1016/j.neuint.2017.05.011. [PubMed: 28527632]

(46). DeCoteau W; Heckman KL; Estevez AY; Reed KJ; Costanzo W; Sandford D; Studlack P; Clauss J; Nichols E; Lipps J; et al. Cerium oxide nanoparticles with antioxidant properties ameliorate strength and prolong life in mouse model of amyotrophic lateral sclerosis. Nanomedicine 2016, 12 (8), 2311–2320. DOI: 10.1016/j.nano.2016.06.009. [PubMed: 27389143]

(47). Najafi R; Hosseini A; Ghaznavi H; Mehrzadi S; Sharifi AM Neuroprotective effect of cerium oxide nanoparticles in a rat model of experimental diabetic neuropathy. Brain Res Bull 2017, 131, 117–122. DOI: 10.1016/j.brainresbull.2017.03.013. [PubMed: 28373151]

(48). Asgharzadeh F; Hashemzadeh A; Rahmani F; Yaghoubi A; Nazari SE; Avan A; Mehr SMH; Soleimanpour S; Khazaei M Cerium oxide nanoparticles acts as a novel therapeutic agent for ulcerative colitis through anti-oxidative mechanism. Life Sci 2021, 278, 119500. DOI: 10.1016/j.lfs.2021.119500. [PubMed: 33862111]

(49). Greenough MA; Camakaris J; Bush AI Metal dyshomeostasis and oxidative stress in Alzheimer's disease. Neurochem Int 2013, 62 (5), 540–555. DOI: 10.1016/j.neuint.2012.08.014. [PubMed: 22982299] Tonnies E; Trushina E Oxidative Stress, Synaptic Dysfunction, and Alzheimer's

Disease. J Alzheimers Dis 2017, 57 (4), 1105–1121. DOI: 10.3233/JAD-161088. [PubMed: 28059794]

(50). Hirst SM; Karakoti AS; Tyler RD; Sriranganathan N; Seal S; Reilly CM Anti-inflammatory properties of cerium oxide nanoparticles. Small 2009, 5 (24), 2848–2856. DOI: 10.1002/smll.200901048. [PubMed: 19802857]

(51). Coraci IS; Husemann J; Berman JW; Hulette C; Dufour JH; Campanella GK; Luster AD; Silverstein SC; El-Khoury JB CD36, a class B scavenger receptor, is expressed on microglia in Alzheimer's disease brains and can mediate production of reactive oxygen species in response to beta-amyloid fibrils. Am J Pathol 2002, 160 (1), 101–112. DOI: 10.1016/s0002-9440(10)64354-4. [PubMed: 11786404] Bao Y; Qin L; Kim E; Bhosle S; Guo H; Febbraio M; Haskew-Layton RE; Ratan R; Cho S CD36 is involved in astrocyte activation and astroglial scar formation. J Cereb Blood Flow Metab 2012, 32 (8), 1567–1577. DOI: 10.1038/jcbfm.2012.52. [PubMed: 22510603]

(52). Huang MY; Tu CE; Wang SC; Hung YL; Su CC; Fang SH; Chen CS; Liu PL; Cheng WC; Huang YW; et al. Corylin inhibits LPS-induced inflammatory response and attenuates the activation of NLRP3 inflammasome in microglia. BMC Complement Altern Med 2018, 18 (1), 221. DOI: 10.1186/s12906-018-2287-5. [PubMed: 30107806] Lin Z; Chen C; Yang D; Ding J; Wang G; Ren H DJ-1 inhibits microglial activation and protects dopaminergic neurons in vitro and in vivo through interacting with microglial p65. Cell Death Dis 2021, 12 (8), 715. DOI: 10.1038/s41419-021-04002-1. [PubMed: 34274951]

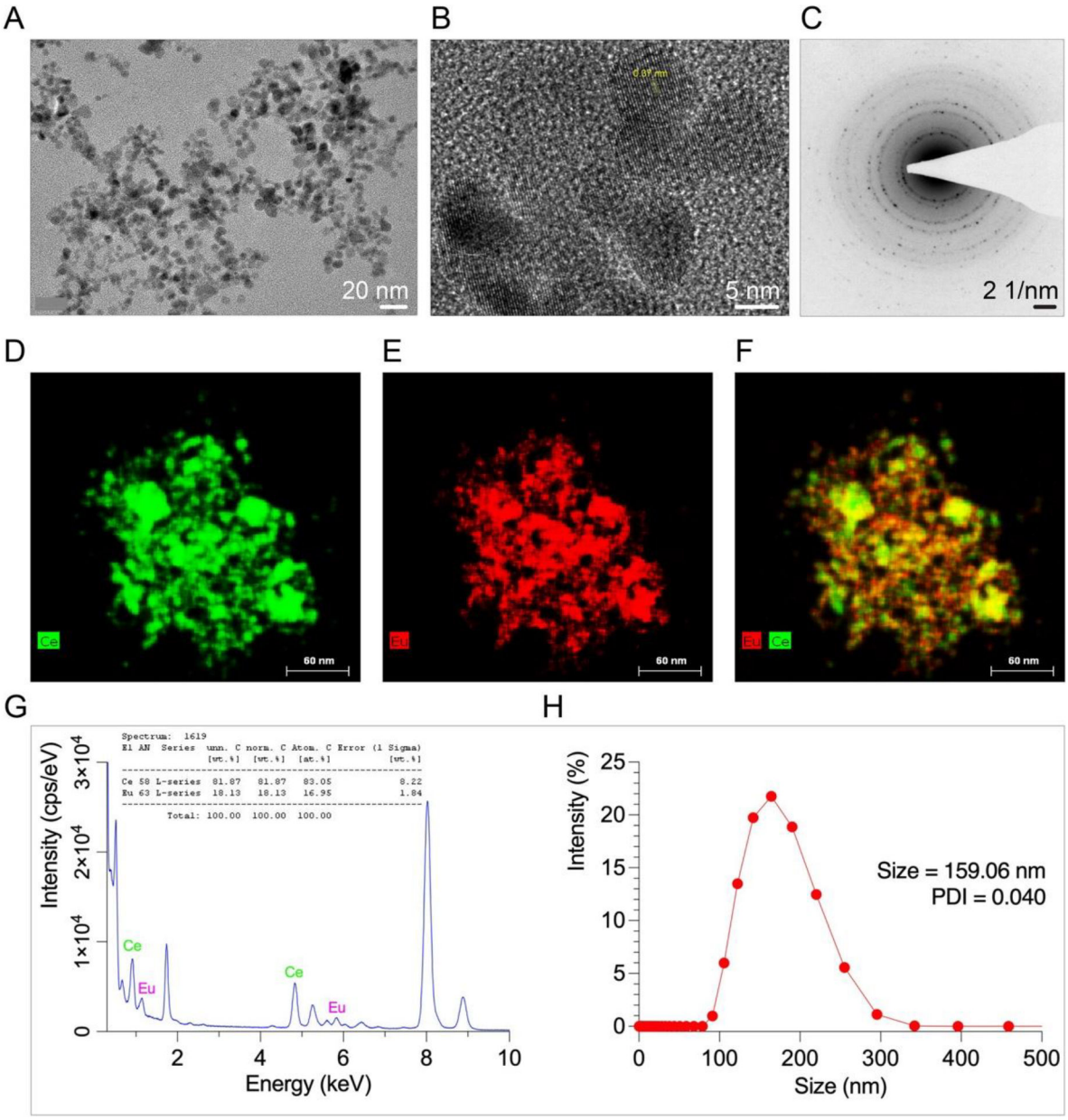

Figure 1. EuCeO$_2$NPs characterization

; (A) TEM image of particles with uniform size and shape. (B) HR-TEM image of EuCeO$_2$NPs crystal structure with lattice pattern shows high crystalline structure. HR-TEM image reconstruction where d=0.37 nm indicates characteristic interlattice spacing of cerium oxide nanoparticles. HR-TEM data corresponds to (C) Selected Area Electron Diffraction Pattern (SAED) identifying crystalline phase of EuCeO$_2$NPs structure. (D-F) STEM maps of EuCeO$_2$NPs demonstrated bimetallic composition of EuCeO$_2$NPs and even distribution of cerium and europium ions in merged STEM images. (G) EDX spectra of EuCeO$_2$NPs clearly shows presence of Ce and Eu in the sample with 81.87% Ce and 18.13% Eu-doped in the Ce structure. (H) Size distribution analysis by dynamic light scattering (DLS). Lipid

coated $EuCeO_2$NPs were dispersed in deionized water and their DLS analysis revealed that the synthesized nanoparticles had an average size of 159.06 nm with 0.04 PDI.

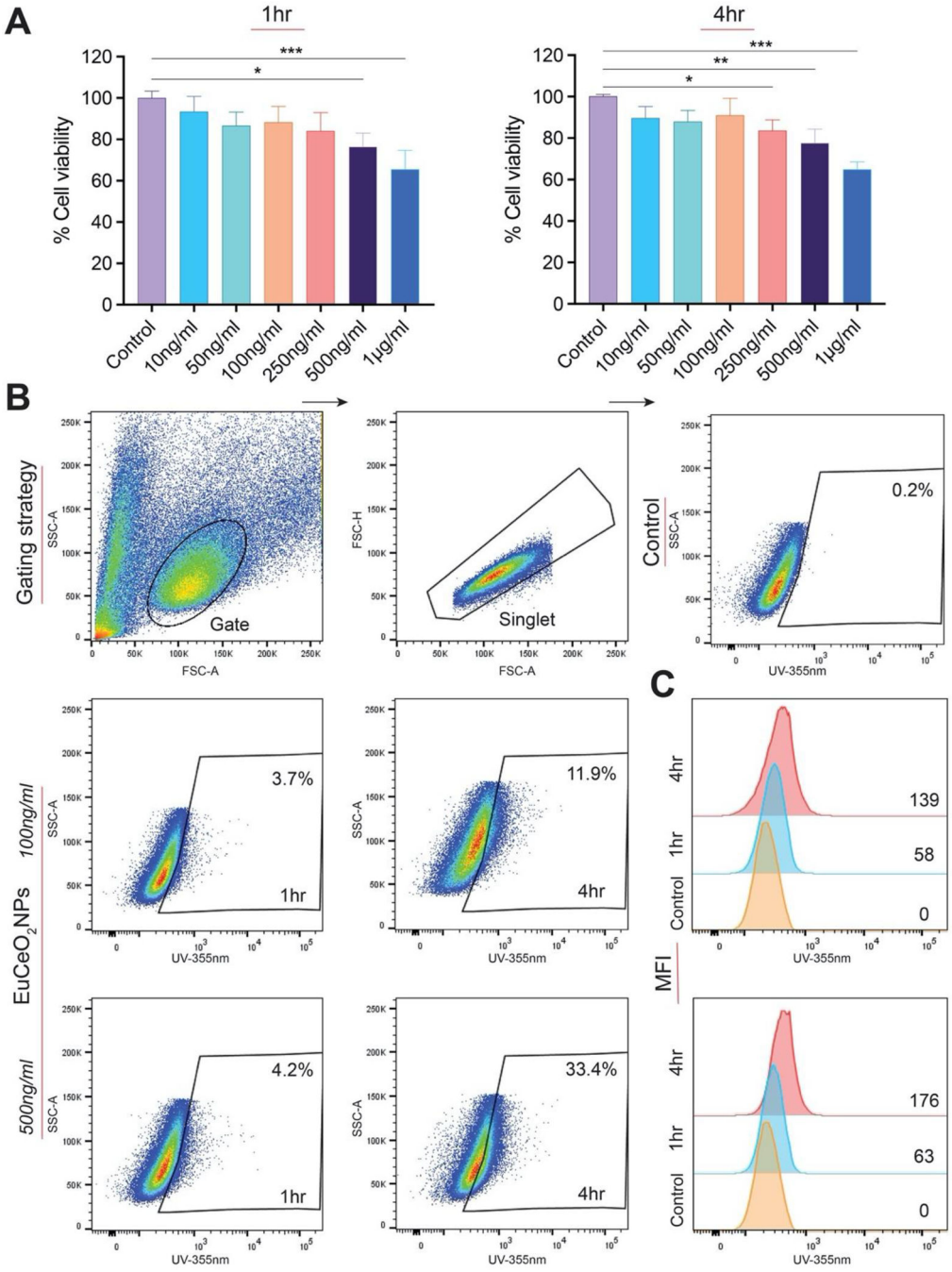

Figure 2. EuCeO$_2$NP and BV2 cells.

(A) BV2 cells were treated with EuCeO$_2$NPs for 1 and 4 hr at different concentrations. Cell vitality was measured by the MTT assay (n = 4). One-way ANOVA followed by Newman–Keuls post-hoc test was used to determine statistical significance. *$p < 0.05$, **$p < 0.01$, ***$p < 0.001$. (B) BV2 cells were treated with EuCeO$_2$NPs at two different concentrations (100 and 500 ng/ml) and cells were incubated for either 1 or 4 hr followed by flowcytometric analysis of nanoparticle cellular uptake. (C) Mean fluorescence intensity

(MFI) was quantified and plotted to represent europium uptake in BV2 cells following $EuCeO_2$NP treatment.

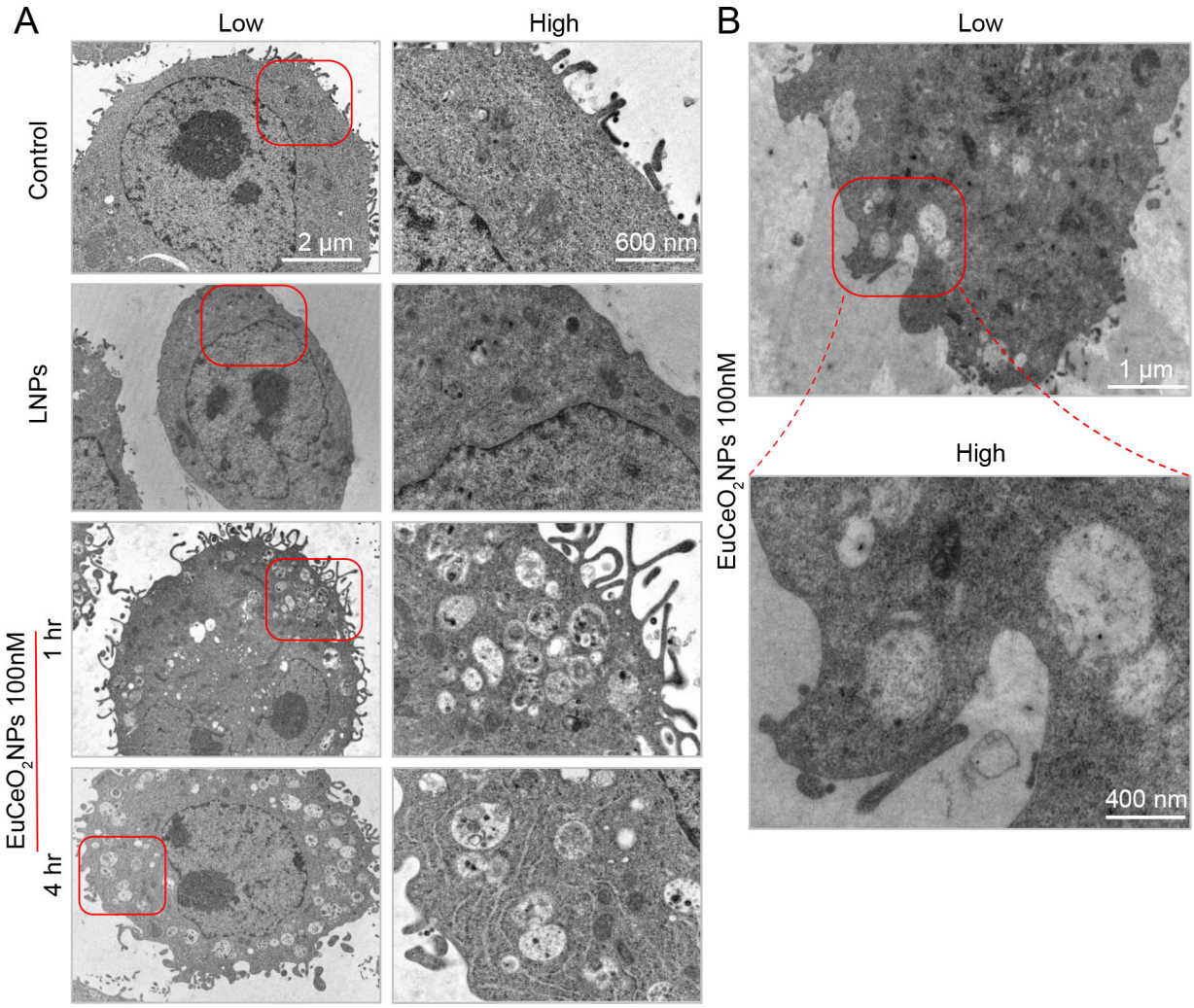

Figure 3. Lipid-coated $EuCeO_2$NPs facilitate BV2 phagocytosis visualized by transmission electron microscopy (TEM).

(A) Low and high magnification images of fixed BV2 cells from either untreated (control) or 100 ng/ml LNPs or $EuCeO_2$NPs treated cells were observed for nanoparticle uptake after 1 and 4 hr of treatment. (B) $EuCeO_2$NPs treated BV2 cells demonstrated nanoparticle phagocytosis following 1hr incubation.

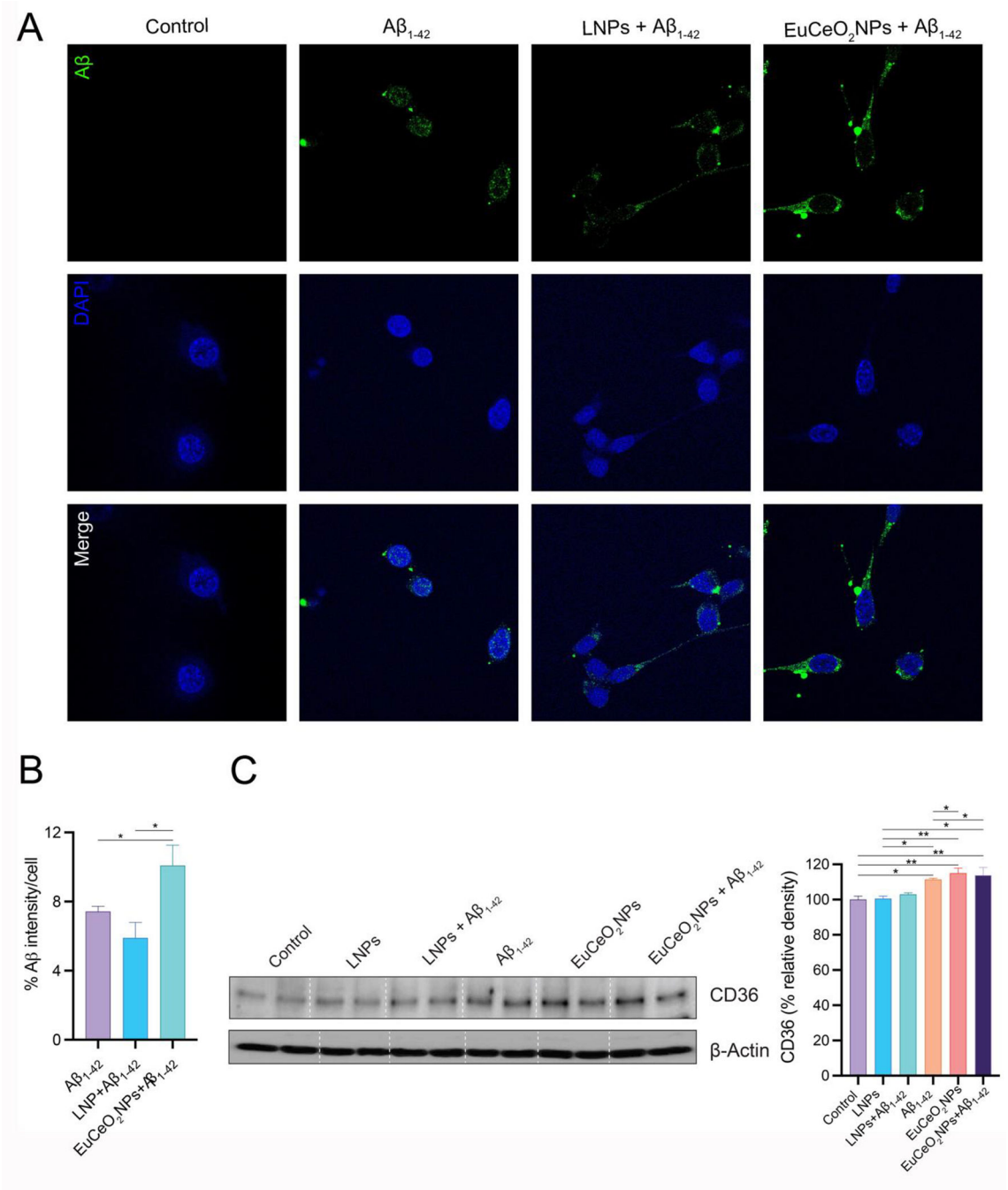

Figure 4. EuCeO$_2$NPs facilitate Aβ uptake in BV2 cells.

(a) BV2 cells treated with either EuCeO$_2$NPs (100 ng/ml) or LNPs for 1 hr followed by A$\beta_{1–42}$ (10 μM) exposure for additional hr and visualized using intracellular immunofluorescence staining. Immunofluorescent images of Aβ (green), nuclear stain DAPI (blue) and merged images are shown. Scale bar=10 μm. (B) Dense intensity of Aβ fluorescence was measured using ImageJ software. Experiments were performed in triplicate. One-way ANOVA followed by Newman–Keuls post-hoc test was used to determine statistical significance. *$p < 0.05$. (C) Immunoblot images of CD36 normalized

to β-actin expression in BV2 cells after sequential $EuCeO_2$NPs and $A\beta_{1-42}$ treatment. Densitometric quantification of CD36 expression was performed using ImageJ software. n = 4. One-way ANOVA followed by Newman–Keuls post-hoc test was used to determine statistical significance. *$p < 0.05$, **$p < 0.01$.

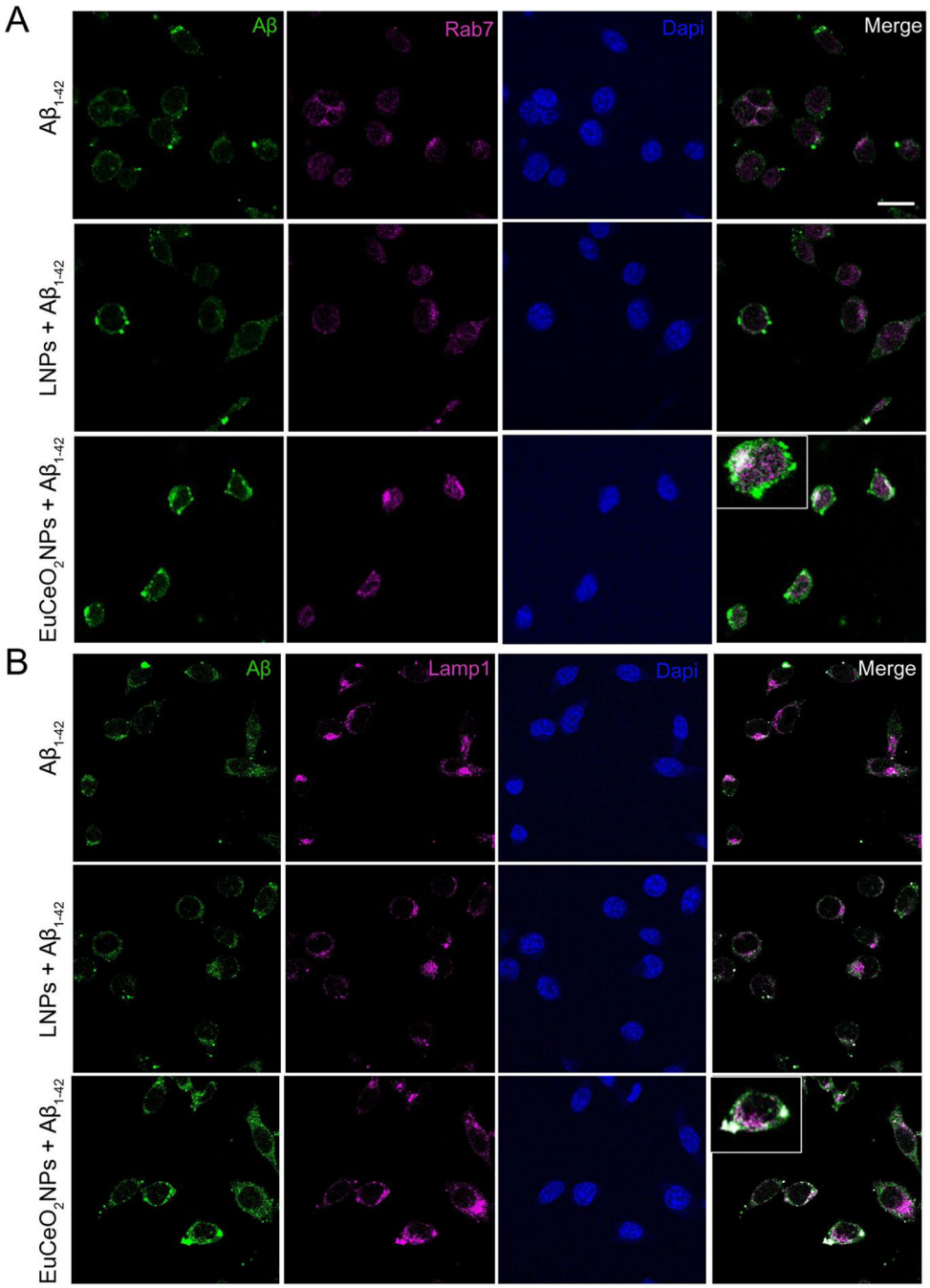

Figure 5. EuCeO$_2$NPs effect Aβ endolysosomal trafficking.

Confocal microscopic images captured after sequential treatments of EuCeO$_2$NPs and Aβ$_{1–42}$ of BV2 cells and co-localization of Aβ with late endosomal marker Rab7 (A) and lysosomal marker LAMP-1 (B) is shown in merged images. Scare bar = 10 μm. Cell with high co-localization area is shown as insert in EuCeO$_2$NPs plus Aβ$_{1–42}$ treated group.

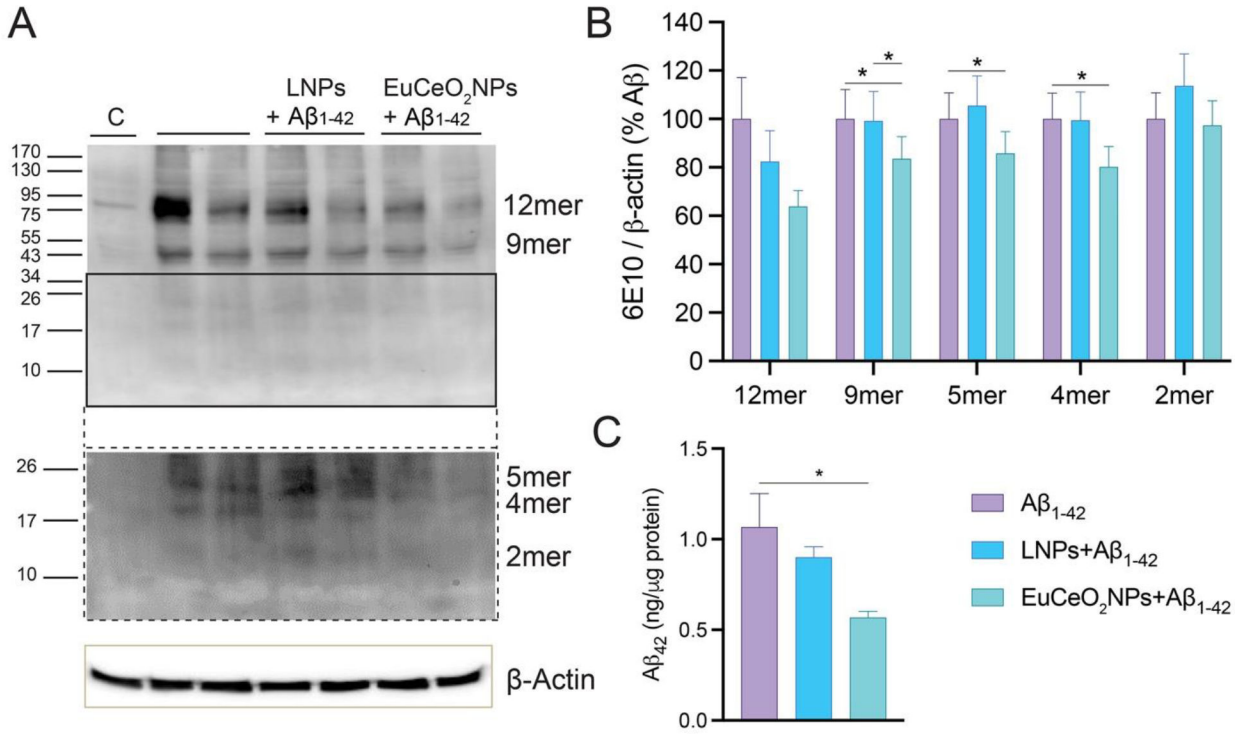

Figure 6. EuCeO$_2$NPs effects on BV2 Aβ metabolism.

(A) BV2 cells treated with EuCeO$_2$NPs (100 ng/ml) followed by A$\beta_{1–42}$ (10 μM) exposure for additional 4 hr. After incubation, cells were harvested for immunoblot analysis using 10% SDS-polyacrylamide Tris-Tricine gel and 6E10 antibody. Membrane image was captured after low (top) and high (bottom) exposure times to the substrate. (B) Expression of different Aβ oligomers was quantified using ImageJ software. (C) The amount of soluble A$\beta_{1–42}$ in cell lysates was quantified using ELISA. n = 4. One-way ANOVA followed by Newman–Keuls post-hoc test was used to determine statistical significance. *$p < 0.05$.

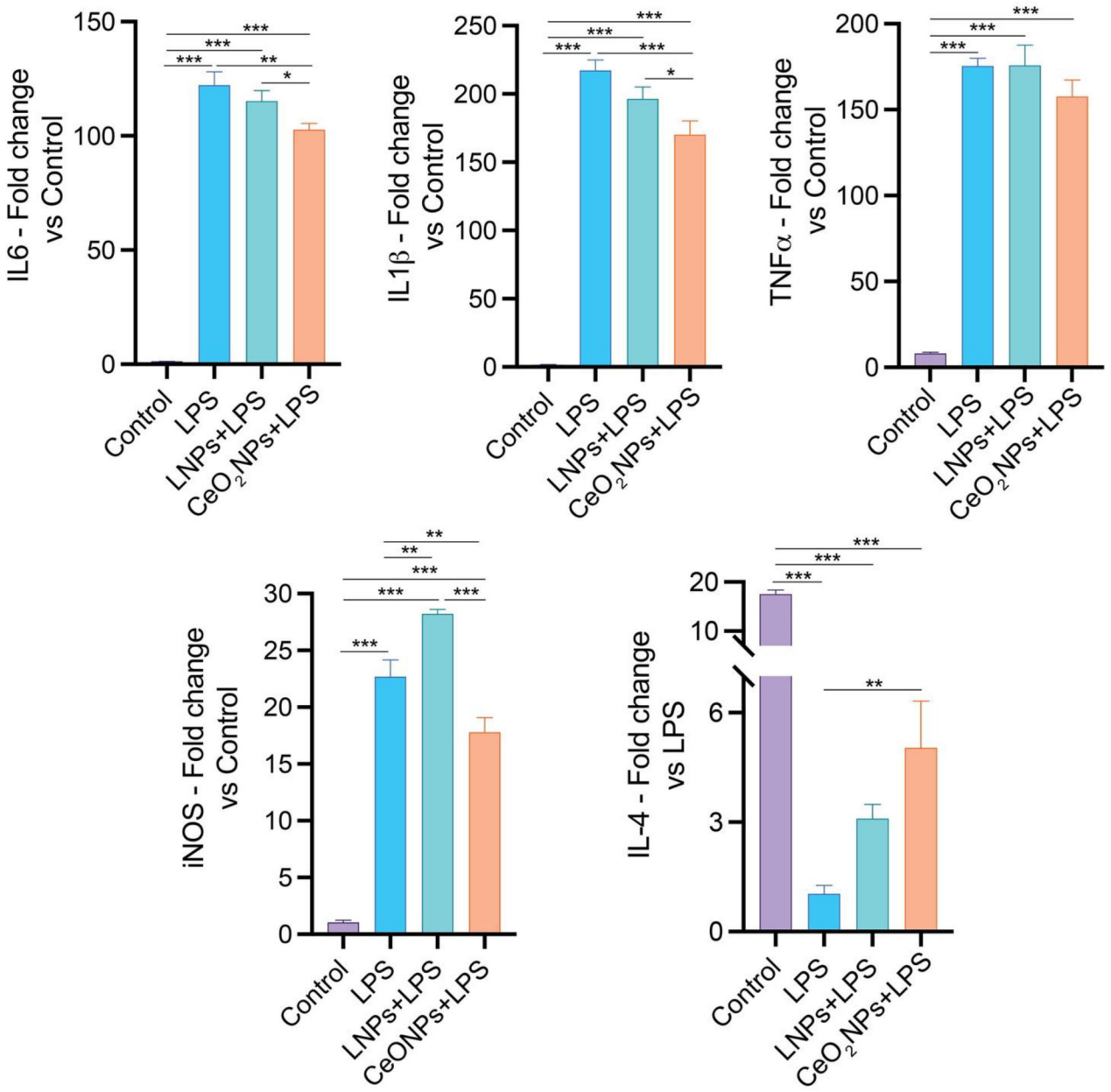

Figure 7. EuCeO$_2$NPs reduce BV2 inflammatory activities.

BV2 cells treated with LPS (0.5 μg/ml) for 4 hr in absence and presence of EuCeO$_2$NPs (100 ng/ml) or LNPs and after incubation, different inflammatory cytokine (IL-6, IL-1β, TNF-α, and IL-4) and classical activation marker iNOS levels were measured using gene-specific primers and RT^2-qPCR assay. n = 6. One-way ANOVA followed by Newman–Keuls post-hoc test was used to determine statistical significance. *$p < 0.05$, **$p < 0.01$, ***$p < 0.001$.